Colony-stimulating factor CSF2 mediates the phenotypic plasticity of small-cell lung cancer by regulating the p-STAT3/MYC pathway

HUI LI[1-3*], RUI ZHONG[1,2*], CHUNYING HE[3], CHENCHEN TANG[3], HERAN CUI[3], RIXIN LI[3], YAN LIU[1,2], SHAOWEI LAN[1,2] and YING CHENG[1,2,4]

[1]Translational Cancer Research Lab; [2]Jilin Provincial Key Laboratory of Molecular Diagnostics for Lung Cancer, [3]Biobank and [4]Department of Medical Thoracic Oncology, Jilin Cancer Hospital, Changchun, Jilin 130000, P.R. China

Received December 31, 2021; Accepted April 20, 2022

DOI: 10.3892/or.2022.8333

Abstract. Relapse and drug resistance are the main causes of mortality in patients with small-cell lung cancer (SCLC). Intratumoral heterogeneity (ITH) is a key biological mechanism that leads to relapse and drug resistance. Phenotypic plasticity is an important factor that leads to ITH in SCLC, although its mechanisms and key regulatory factors remain to be elucidated. In the present study, cell proliferation and cell switch assay were measured using trypan blue. Alamar Blue was used to test drug sensitivity. Differential genes were screened by RNA sequencing. Reverse transcription-quantitative PCR and western blotting were performed to assess the expressions of CSF2/p-STAT3/MYC pathway related molecules, neuroendocrine (NE)/non-neuroendocrine (non-NE), transcription factors and drug-related targets. The present study found that SCLC cell line NCI-H69 exhibited adherent (H69A) and suspensive (H69S) phenotypes, which could switch back and forth. The two phenotypic cells had significant differences in cellular NE and non-NE characteristics, drug sensitivity and expression of drug-related targets. RNA sequencing showed that granulocyte-macrophage colony-stimulating factor [i.e., colony-stimulating factor 2 (CSF2)] was the main differentially expressed gene between the two phenotypes and that H69A cells highly expressed CSF2. The inhibition of CSF2 promoted the transformation from H69A to H69S, increased drug sensitivity and NE marker expression and decreased the non-NE marker expression in H69A. The STRING, Pathway Commons and Reactome databases showed a potential regulatory relationship between CSF2 and phosphorylated signal transducer and activator of transcription 3 (p-STAT3)/MYC. p-STAT3 and MYC expression was higher in H69A cells than in H69S cells and CSF2 silencing inhibited their expression. Taken together, these results indicated that CSF2 may regulate the phenotypic plasticity of SCLC through the phosphorylated STAT3/MYC pathway, thereby limiting the transformation between cell clones with different phenotypes and changing the sensitivity of specific cell clones to targeted drugs. Targeting CSF2 may be a potential therapeutic strategy to overcome drug resistance in SCLC treatment by influencing ITH.

Correspondence to: Professor Ying Cheng, Translational Cancer Research Lab, Jilin Cancer Hospital, 1066 Jinhu Road, Changchun, Jilin 130000, P.R. China
E-mail: chengying@csco.org.cn

*Contributed equally

Abbreviations: SCLC, small cell lung cancer; PCR, polymerase chain reaction; RT-qPCR, reverse transcription quantitative PCR; NE, neuroendocrine; CSF2, colony-stimulating factor 2; ASCL1, achaete-scute homologue 1; NEUROD1, neurogenic differentiation factor 1; YAP1, YES-associated protein 1; POU2F3, POU class 2 homeobox 3; NSCLC, non-small cell lung cancer; CTCs, circulating tumor cells; ITH, intratumoral heterogeneity; MDSCs, myeloid-derived suppressor cells; VEGFR, vascular endothelial growth factor receptor; PDGFR, platelet-derived growth factor receptor; FGFR, fibroblast growth factor receptors; c-Kit, stem cell factor receptor; CSF1R, colony-stimulating factor 1 receptor; SYP, synaptophysin; EGFR, epidermal growth factor receptor; ALK, anaplastic lymphoma kinase; ROS1, ROS proto-oncogene 1; TKI, tyrosine kinase inhibitor; FC, fold change; GO, Gene Ontology; KEGG, Kyoto Encyclopedia of Genes and Genomes; DEG, differentially expressed genes; OD, optical density; SDS, sodium dodecyl sulfate; mTOR, mammalian target of rapamycin; OS, overall survival

Key words: small cell lung cancer, granulocyte-macrophage colony-stimulating factor, intratumoral heterogeneity, phenotypic plasticity, drug resistance

Introduction

Small-cell lung cancer (SCLC) accounts for ~15% of all lung cancers and is one of the most lethal diseases with a 5-year survival of 1-5% in extensive-stage (ES)-SCLC (1-3). Most patients with SCLC are sensitive to platinum-based first-line chemotherapy, although a number of patients develop drug resistance and rapid relapse (4), which is attributed to the presence of cell heterogeneity in SCLC and the patients eventually succumb (5). Intratumoral heterogeneity (ITH) is a characteristic of different tumor cell clones from the same

tumor tissue. ITH is also reflected by genetic, functional and phenotypic differences. SCLC presents with different growth patterns: The more common 'classic' subtype, which grows predominantly as spherical aggregates of floating cells and the 'variant' subtype, which grows as loosely adherent aggregates or as a more tightly adherent monolayer in cell culture (6). Expression profiling of these distinct populations suggests that the floating phenotype has the more typical epithelial neuroendocrine (NE) features, whereas the adherent phenotype has a more non-neuroendocrine (non-NE) expression profile (6,7). The paracrine signaling pathway regulates the crosstalk between NE and non-NE that can change tumor cell behavior (8,9). SCLC subtypes are defined by four transcription regulators: Achaete-scute homologue 1 (ASCL1; also known as ASH1) for SCLC-A, neurogenic differentiation factor 1 (NeuroD1) for SCLC-N, POU class 2 homeobox 3 (POU2F3) for SCLC-P and YES-associated protein 1 (YAP1) for SCLC-Y (10). SCLC-A and SCLC-N are NE subtypes and SCLC-Y and SCLC-P are non-NE subtypes (11). The phenotypic difference in SCLC is the key factor that leads to the formation of ITH, but its biological function and mechanism are unclear and require clarification.

Phenotypic plasticity, which is the ability of cells to change from one phenotype to another, is a mechanism responsible for phenotypic differences. In the formation of ITH, phenotypic plasticity is the source of ITH formation and the mechanism that leads to differences in drug sensitivity and acquired drug resistance (10). Treatment-induced stress or hypoxia has an important role in NE transformation (10,12,13), which can promote breast cancer, pancreatic cancer and other tumor cells to adapt to an environment that influences epithelial-mesenchymal transition (EMT) (13,14). In NE cells, MYC upregulates NOTCH2, Hes1, Hes6 and Jag2 expression and activates Notch to dedifferentiate tumor cells, thereby promoting a temporal shift in SCLC from SCLC-A to SCLC-N to SCLC-Y (15). In this process, cells change from 'classic' (i.e., NE) tight, round, spherical aggregates to 'variant' (i.e., non-NE) chain-link amorphous cell colonies. Regulating MYC expression may alter cell fate, morphology and drug sensitivity (15).

Granulocyte-macrophage colony-stimulating factor (GM-CSF), also called colony-stimulating factor 2 (CSF2), is secreted by different types of cells (e.g., activated T cells, B cells, macrophages, mast cells, vascular endothelial cells, fibroblasts and a wide variety of cancer cell types) and is primarily involved in immune activation and regulating the function of inflammatory cytokines. Under appropriate stimulation, CSF2 is also secreted by a number of nonimmune cells (16) and it regulates the growth, invasion and migration of tumor cells such as human melanoma, skin cancer and colorectal cancer in an autocrine or paracrine manner (11,17,18). One report (19) demonstrates that myeloid-derived suppressor cells (MDSC) can upregulate MYC expression by inducing the CSF2/phosphorylated signal transducer and activator of transcription 3 (p-STAT3) signaling pathway to promote epithelial ovarian cancer cell stemness. The inhibition of STAT3 can significantly reduce cell adherence ability (20) and the expression of EMT-related proteins and the non-NE marker CD44 (21). However, whether CSF2, p-STAT3 and MYC are involved in the phenotypic plasticity of SCLC is unclear. The aim of the present study was to identify the biological function and mechanism of CSF2 in regulating SCLC phenotypic plasticity and to verify whether CSF2 regulated SCLC phenotypic plasticity through p-STAT3/MYC signaling pathway to drive ITH and cause relapse and drug resistance.

Materials and methods

Cell culture. The human SCLC cell line NCI-H69 was purchased from Cell Resource Center at the Institute of Basic Medical Sciences of the Chinese Academy of Medical Sciences/Peking Union Medical College (Beijing, China). NCI-H69 exhibited adherent (H69A) and suspensive (H69S) phenotypes. H69S cells in the supernatant were separated by centrifugation (200 x g for 5 min at 22-24˚C) for cell passaging. H69A cells had to be detached by treatment with 0.02% ethylenediaminetetraacetic acid (EDTA; MilliporeSigma) for subcultivation. The two of them of them were cultured in RPMI 1640 medium, supplemented with 10% fetal bovine serum and 100 U/ml penicillin and streptomycin (all from Gibco; Thermo Fisher Scientific, Inc.) at 37˚C in a 5% CO_2 incubator.

Cell transfection. CSF2 shRNA short hairpin (sh) RNA and negative control were synthesized by Genechem, Inc. The CSF2 shRNA sequence was: 5'-CCCAGATTATCACCTTTG AAA-3'. The negative control sequence was non-targeting sequence: 5'-TTCTCCGAACGTGTCACGT-3'. Briefly, $1x10^6$ cells (H69A) per well were seeded in 6-well plates the day before transfection. After 24 h, the cells were resuspended in 100 μl of Buffer R, then gently mix with 5 μg of negative control or CSF2 shRNA; 100 μl of the cells mixed with negative control or CSF2 shRNA complexes were pipetted into the 3 ml Buffer E2. The Neon System (Thermo Fisher Scientific, Inc.) was used for electroporation; 1,300 V/20 ms/2 pulses were used for electroporation at 22-24˚C. After 48 h, the cells were used for the subsequent experiments.

Ribonucleic acid extraction and library preparation. Total RNA was extracted by using TRIzol® reagent (Thermo Fisher Scientific, Inc.), following the manufacturer's procedure. A total of 3 μg RNA per sample was used as the input material for preparation of the RNA-Seq library. mRNA was purified from total RNA by using poly-T oligo-attached magnetic beads. Fragmentation was carried out using divalent cations at 22-24˚C in NEB Next First Strand Synthesis Reaction Buffer (5X; New England BioLabs, Inc.). First strand complementary deoxyribonucleic acid (cDNA) was synthesized using a random hexamer primer and M-MuLV and Solutions Reverse Transcriptase (RNase H). Second-strand cDNA synthesis was subsequently conducted by using DNA polymerase I and RNase H. The remaining overhangs were converted to blunt ends via exonuclease/polymerase activities. After adenylation of the 3' ends of the DNA fragments, NEBNext Adaptor (New England BioLabs, Inc.) with hairpin loop structures were ligated to prepare for hybridization. To select cDNA fragments of preferentially 250-300 bp in length, the library fragments were purified with the AMPure XP system (Beckman Coulter, Inc.). Then 3 μl of USER Enzyme (New England BioLabs, Inc.) were thereafter used to generate size-selected, adaptor-ligated cDNA at 37˚C for 15 min, followed by 5 min at 95˚C before polymerase chain reaction (PCR). PCR was conducted using

Phusion High-Fidelity DNA polymerase, universal PCR primers and an Index (X) primer. Finally, the PCR products were purified (AMPure XP system; Beckman Coulter, Inc.) and the quality of the library was evaluated on the Agilent Bioanalyzer 2100 system (Agilent Technologies, Inc.).

Quality control and read mapping to the reference genome. Quality score (Q)20, Q30 and the guanine-cytosine (GC) content of the clean data were calculated. All downstream analyses were based on clean data of high quality. The reference genome and gene model annotation files were downloaded directly from the genome website (https://www.gencodegenes.org/human/releases.html). Paired-end clean reads were aligned to the reference genome using STAR v20201 (https://github.com/alexdobin/STAR). STAR was selected as the mapping tool because it can generate a more precise database of uniquely mapped reads, compared to other mapping tools.

Quantification of gene expression level. Cufflinks v2.2.1 (https://github.com/cole-trapnell-lab/cufflinks) was used to count the number of reads assigned to each gene. The fragments per kilobase of transcript sequence per millions (FPKM) of each gene were then calculated, based on the length of the gene and the read count mapped to this gene. The calculation of FPKM took into account the effect of sequencing depth and gene lengths for the reads count. This is the most used method for estimating the level of gene expression.

Differential expression analysis. Differential gene expression analysis was conducted using Cufflinks v2.2.1. The resulting P-values were adjusted by using the Benjamini and Hochberg approach to control the false discovery rate (22,23). A P-value of 0.05 and an absolute fold change (FC) of 1.5 were set as the thresholds for a significant differential expression. Gene Ontology (GO) and Kyoto Encyclopedia of Genes and Genomes (KEGG) enrichment analyses of differentially expressed genes (DEG) was implemented by the cluster Profiler R package (https://mirrors.tuna.tsinghua.edu.cn/CRAN/bin/windows/base/old/4.0.3/) in which gene length bias was corrected. GO terms with a corrected P-value <0.05 were considered significantly enriched by DEG. KEGG is a database resource for understanding high-level functions and utilities of a biological system such as the cell, the organism and the ecosystem, based on molecular-level information, especially large-scale molecular datasets generated by genome sequencing and other high throughput experimental technologies (http://www.genome.jp/kegg/). The cluster Profiler R package was used to test the statistical enrichment of differential expression genes in the KEGG pathways.

Reverse transcription-quantitative (RT-q) PCR. Cells were seeded in a 6-well microplate at a density of $5x10^5$ cells per well. Total RNA was extracted using the RNA mini kit (Qiagen, Inc.) according to the manufacturer's protocols and the optical density (OD) 260/280 nm ratio was >1.95. Reverse transcription was conducted using a reverse transcription kit (Takara Bio, Inc.). The samples were analyzed by using RTqPCR on a LightCycler 480 system (Roche Diagnostics) with the SYBR Green Master mix kit (Takara Bio, Inc.) with the following conditions: 95˚C for 3 min, followed by 40 cycles at 95˚C for 30 sec, 57˚C for 30 sec and 72˚C for 30 sec. Glyceraldehyde-3-phosphate dehydrogenase (GAPDH) mRNA was used to normalize the relative amount of mRNA. The following primers were used: vascular endothelial growth factor receptor (VEGFR): forward, 5'-ACCATACCTCCT GCGAAACC-3' and reverse, 5'-CGGGGACACCATTAG CATGA-3'; platelet-derived growth factor receptor (PDGFR): forward, 5'-GAGACTGTTGGGCGAAGGTT-3' and reverse, 5'-TGGGTGGTCACTCCTCAGAA-3'; fibroblast growth factor receptor (FGFR): forward, 5'-TCAGATGCTCTCCCC TCCTC-3' and reverse, 5'-ACGGGGTTTGGTTTGGTG TT-3'; stem cell factor receptor (c-Kit): forward, 5'-ACTTGG AGCCTGCACCATT-3' and reverse, 5'-CTATCGCTGCAG GAAGACTC-3'; Aurora B: forward, 5'-ACCTGCACCATC CCAACATC-3' and reverse, 5'-ATGATCGTGGCTGTTCGC TG-3'; colony-stimulating factor 1 receptor (CSF1R): forward, 5'-TATGTCAAAGACCCTGCCCG-3' and reverse, 5'-AAG GAGTAGTTGGTGTGGCG-3'; and GAPDH: forward, 5'-ACCACAGTCCATGCCATCAC-3' and reverse, 5'-TCC ACCACCCTGTTGCTGTA-3'. The relative quantification of the PCR product was calculated, using the $2^{-\Delta\Delta Cq}$ method (24).

Drug sensitivity assay. The drug sensitivity assay was assessed, by using Alamar Blue reagent (cat. no. DAL1100; Invitrogen; Thermo Fisher Scientific, Inc.). H69A and H69S cells were seeded in 96-well plates at a density of 6,000 cells per well and incubated at 37˚C with 5% CO_2 for 48 h in various concentrations of cisplatin (range, 0-10 μg/ml; Selleck, Inc.), etoposide (range, 0-16 μg/ml, Selleck, Inc.), anlotinib (range, 0-6 μg/ml; Chia Tai Tianqing Pharmaceutical Group Co., Ltd.), CS2164 (range, 0-10 μg/ml; Shenzhen Chipscreen Biosciences Co., Ltd.) and RAD001 (range, 0-20 μg/ml; Selleck, Inc.) to obtain the inhibitory concentration values.

Cell proliferation and cell switch assay. H69A and H69S cells were seeded in a 24-well microplate at a density of $1x10^4$ cells per well. For the cell proliferation assay, cells were cultured for 48 h and then stained with 0.4% trypan blue for 1 min at 22-24˚C. Countstar (ALIT Biotech Co., Ltd.) was used to count cell numbers. For the cell switch assay, adherent cells and cell suspensions were collected from H69A cells and H69S cells, respectively, after being cultured for 24 and 48 h, respectively. They were then stained with 0.4% trypan blue for 1 min at 22-24˚C. The number of cells was counted using Countstar. The rate of adherent cells to suspensive cells is the number of adherent cells/(number of adherent cells + number of cells in the suspension). The ratio of cells in suspension to adherent cells=number of cells in suspension/(number of adherent cells + number of suspensive cells).

Western blotting. Cells were harvested and total proteins were extracted using RIPA lysis buffer containing the protease inhibitor phenylmethylsulfonyl fluoride and a cocktail (Roche Applied Science). The supernatant was then transferred to another tube after centrifugation at 15,000 x g at 4˚C for 15 min. The concentration of the protein samples was quantified using a BCA protein assay kit (Takara Bio, Inc.). The lysate was mixed with 5X sodium dodecyl sulfate (SDS) loading buffer (BioTeke, Inc.) and heated to 95˚C for 5 min. From the

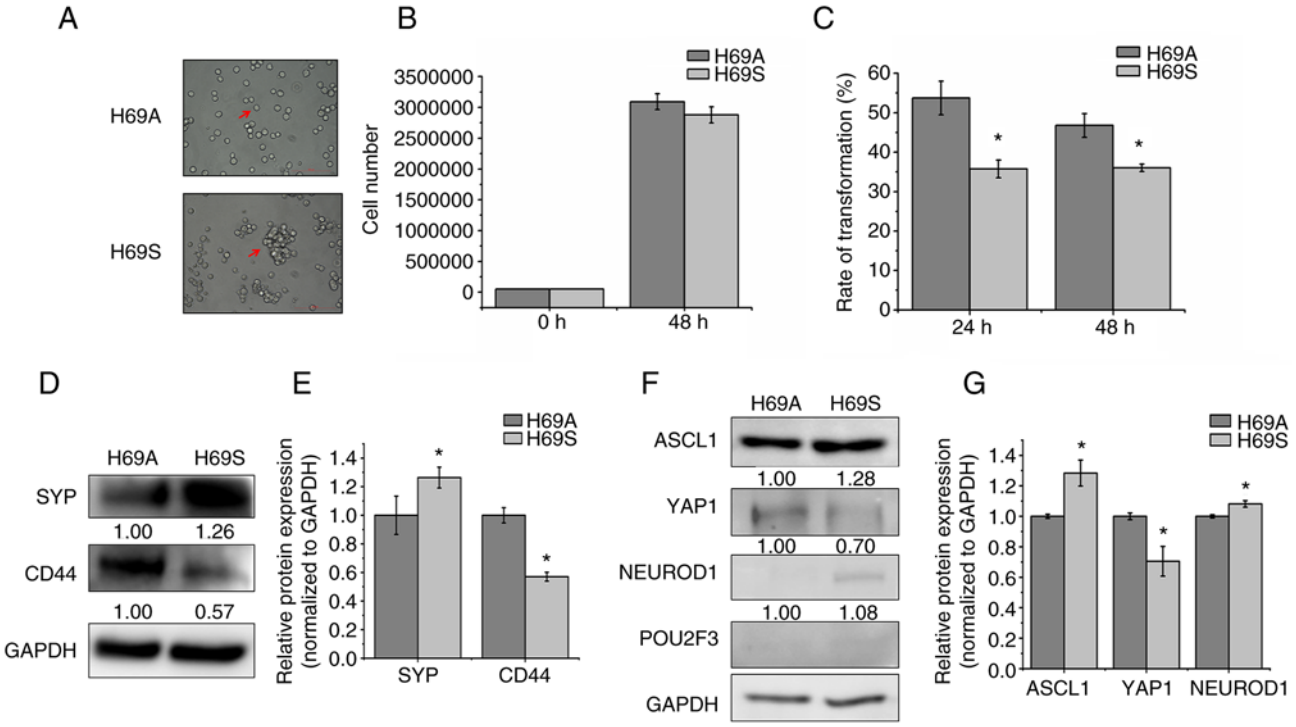

Figure 1. Two distinct phenotypes of SCLC cell line NCI-H69. (A) The arrows indicated the bright-field images of H69A and H69S cells. Magnification, x200. (B) H69A and H69S cells were cultured for 48 h and then stained with trypan blue. Cell proliferation was analyzed using Countstar. (C) H69A and H69S cells were each cultured for 24 and 48 h and then stained with trypan blue. Adherent cells and suspended cells were collected. Cell numbers were counted using Countstar. (D) H69A and H69S cells were collected and western blotting was used to detect the expression of SYP and CD44. GAPDH was the internal standard. (E) Quantitative analysis of (D): H69A was the control (100%). Data are presented as the mean ± standard deviation of three independent experiments. (F) Western blotting was used to detect the expression of ASCL1, NEUROD1, POU2F3, YAP1 and GAPDH. (G) Quantitative analysis of (F): H69A was the control (100%). Data are presented as the mean ± standard deviation of three independent experiments. *P<0.05. SCLC, small cell lung cancer; SYP, synaptophysin; ASCL1, achaete-scute homologue 1; NEUROD1, neurogenic differentiation factor 1; POU2F3, POU class 2 homeobox 3; YAP1, YES-associated protein 1.

total protein, 50 μg was separated using SDS-polyacrylamide gel electrophoresis (SDS-PAGE) on 10% gels and transferred to a polyvinylidene fluoride membrane and then blocked in 5% nonfat milk at 22-24˚C for 1.5 h. It was then incubated overnight at 4˚C with the following primary antibodies: Anti-synaptophysin (anti-SYP; 1:1,000 dilution; cat. no. 4329; Cell Signaling Technology, Inc.), anti-CD44 (1:1,000 dilution; cat. no. 3578; Cell Signaling Technology, Inc.), anti-ASCL1 (1:1,000 dilution; cat. no. ab211327; Abcam), anti-NEUROD1 (1:1,000 dilution; cat. no. ab213725; Abcam), anti-YAP1 (1:1,000 dilution; cat. no. 4912; Cell Signaling Technology, Inc.), anti-POU2F3 (1:200 dilution; cat. no. sc-293402; Santa Cruz Biotechnology, Inc.), anti-p-mammalian target of rapamycin (mTOR; 1:500 dilution; cat. no. 2971; Cell Signaling Technology, Inc.), anti-mTOR (1:500 dilution; cat. no. 2972; Cell Signaling Technology, Inc.), anti-CSF2 (1:1,000 dilution; cat. no. ab56712; Abcam), anti-p-STAT3 (1:1,000 dilution; cat. no. 9145; Cell Signaling Technology, Inc.), anti-STAT3 (1:1,000 dilution; cat. no. 9131; Cell Signaling Technology, Inc.) anti-MYC (1:1,000 dilution; cat. no. 9402; Cell Signaling Technology, Inc.) and anti-GAPDH (1:1,000 dilution; cat. no. ab9485; Abcam). Membranes were then washed and incubated with the corresponding secondary antibodies: Goat antirabbit immunoglobulin G (IgG; 1:3,000 dilution; cat. no. ab6721; Abcam) and goat antimouse IgG (1:3,000 dilution; cat. no. ab6728; Abcam) for 1 h at 22-24˚C. An enhanced chemiluminescent (ECL) kit (MilliporeSigma) was used to detect the proteins. Protein band intensities were quantified by using Quantity One software (version 4.6.9, Bio-Rad Laboratories, Inc.).

Statistical analysis. All data were analyzed by SPSS 17.0 (SPSS, Inc.) and Origin 2021 (Origin Software, Inc.) statistical software. Statistical data are presented as the mean ± standard deviation. The Student's t-test was used to compare the means between two groups, whereas one-way ANOVA was used to compare the means among three or more groups. Dunnett's test for all comparisons are against a single control and Tukey's test for all groups are compared to one another. P-values were based on two-tailed statistical analysis. P<0.05 was considered to indicate a statistically significant difference.

Results

SCLC cell line NCI-H69 grows in two distinct phenotypes. To explore the phenotypic plasticity of SCLC from the same clone, the classic SCLC cell line NCI-H69 was cultured and the adherent cells termed 'H69A' and the suspended cells termed 'H69S.' H69A cell growth presents as a monolayer with a mesenchymal morphology that resembles variant non-NE human SCLC cells, whereas H69S cells have an aggregated growth pattern (Fig. 1A). In general, tumor cells go through anti-anchorage death. To address whether suspended cells had the ability to survive, cell proliferation was tested at 48 h and

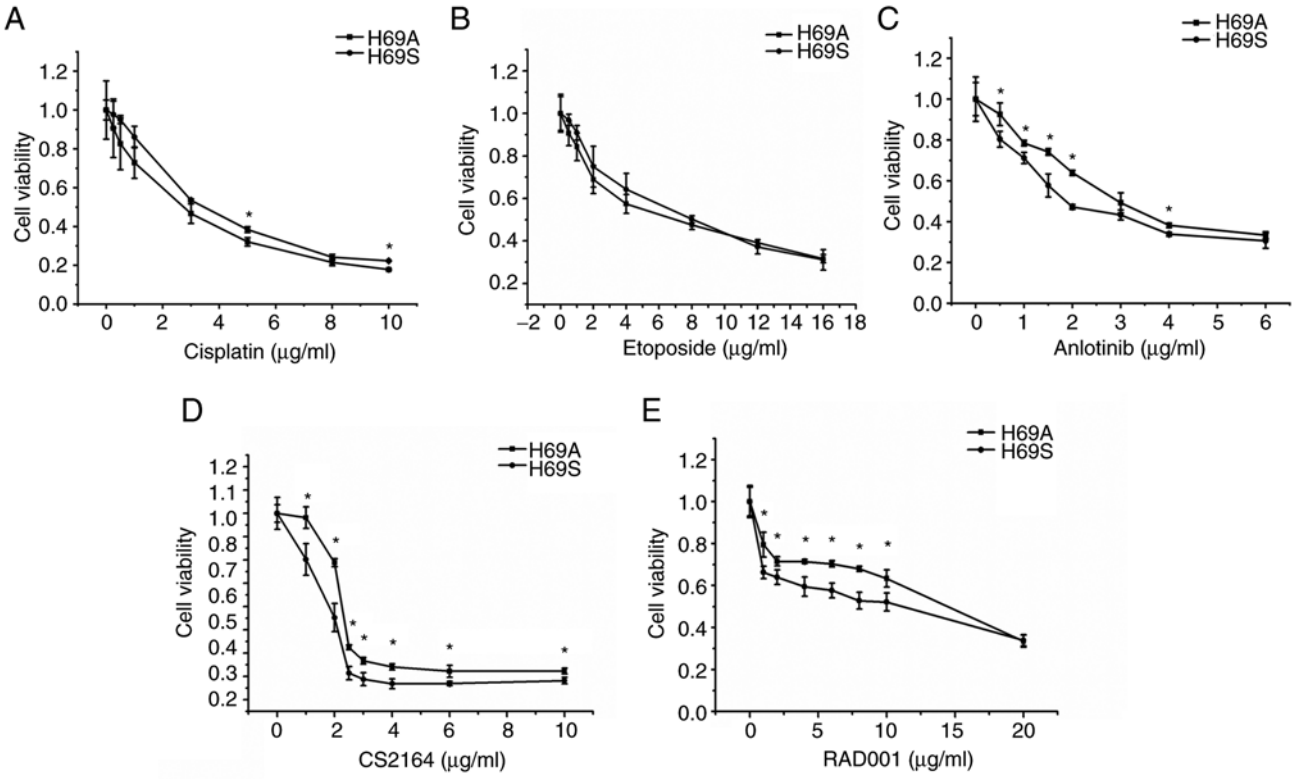

Figure 2. Different drug sensitivities in suspended cells and adherent cells. H69A cells and H69S cells were treated with different concentrations of (A) cisplatin (0, 0.25, 0.5, 1, 3, 5, 8 and 10 μg/ml), (B) etoposide (0, 0.25, 0.5, 1, 3, 5, 8, 12 and 16 μg/ml), (C) anlotinib (0, 0.5, 1, 1.5, 2, 3, 4 and 6 μg/ml), (D) CS2164 (0, 1, 2, 2.5, 3, 4, 6 and 10 μg/ml) and (E) RAD001 (0, 1, 2, 4, 6, 8, 10 and 20 μg/ml) for 48 h. Cell viability was tested using Alamar Blue reagent. All experiments were repeated three times. *P<0.05, vs. adherent group.

no differences found between the two types of cells (Fig. 1B). This finding indicated that the suspended cells did not share the same mechanism of anoikis. To elucidate the relationship between adherent and suspended morphology, the cell switch assay was used to test whether the two cell subtypes could switch back and forth. The results were that H69A and H69S could transform into each other with a transformation rate from H69A cells to H69S cells and from H69S cells to H69A cells of 53.72% vs. 35.72% after 24 h incubation and 46.98% vs. 36.06% after 48 h incubation. This finding indicated that adherent cells may possess a stronger ability to migrate than do suspended cells (Fig. 1C). The detection of NE characteristics and molecular subtypes of adherent and suspended cells showed that the expression level of the non-NE marker CD44 was higher and the expression level of the NE marker SYP was lower in adherent cells than in suspended cells (Fig. 1D and E). H69A and H69S cells strongly expressed ASCL1, but ASCL1 expression was higher in H69S cells than in H69A cells. YAP1 and NEUROD1 expression was lower than that of ASCL1 in H69A and H69S cells. Furthermore, the expression of POU2F3 was faint in the two cell phenotypes (Fig. 1F and G).

Suspended and adherent cells possess heterogeneity with respect to cytotoxicity. Resistance has been attributed to SCLC heterogeneity and a main contributor to ITH is the emergence of multiple clones with genetic variations during tumor progression (25). Therefore, the sensitivity of H69A and H69S to drugs commonly used clinically for SCLC was tested. Commonly used chemotherapy drugs and targeted drugs that have positive results or are receiving greater attention in clinical trials were chosen. H69A and H69S cells were treated with the indicated concentrations of cisplatin, etoposide, anlotinib, CS2164 and RAD001 for 48 h. Inhibitory concentration values were determined by using a cell viability assay in the two cell lines (Fig. 2A-E). Dose-dependent cell survival was observed in H69A and H69S cells. The inhibitory effects of a single drug on the two SCLC cell lines increased with increasing drug concentration. However, the cytotoxic effects of anlotinib, CS2164 and RAD001 were enhanced in H69S cells, compared to H69A cells. The IC_{50}s of anlotinib, CS2164 and RAD001 were 3.09, 3.8 and 17.46 μg/ml, respectively, for H69A and 2.18, 2.09 and 8.48 μg/ml, respectively, for H69S.

Expression of the targeted receptors for anlotinib, CS2164 and RAD001 is higher in the SCLC suspension cells. As the cytotoxicity of anlotinib, CS2164 and RAD001 differed between the H69A and H69S cells, the mechanisms involved were explored. Anlotinib and CS2164 are multitarget inhibitors; therefore, the target receptors VEGFR, PDGFR, FGFR, c-Kit, AuroraB and CSF1R were tested (Fig. 3A). The expression of VEGFR, FGFR and CSF1R was much higher in H69S than in H69A by 7.38, 7.55 and 2.92-fold, respectively. The levels of the RAD001 targets (p-mTOR/mTOR) were also higher in H69S cells than in H69A cells (Fig. 3B and C). Based on these results, it was hypothesized that the levels of targeted receptors against anlotinib, CS2164 and RAD001 could have an important role in the different cytotoxic responses between the two SCLC cells phenotypes.

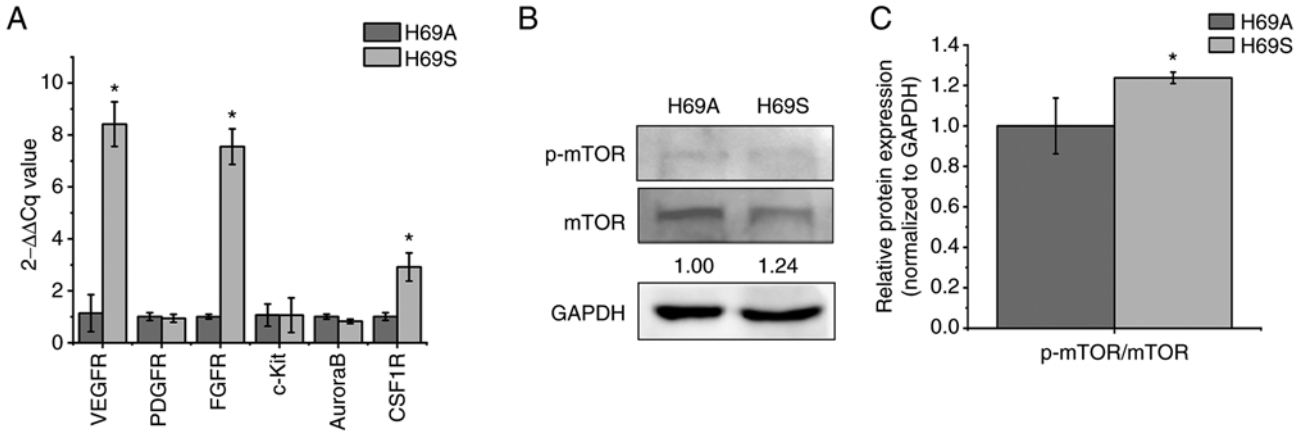

Figure 3. Expression of receptors targeted by anlotinib, CS2164 and RAD001 in H69S cells and H69A cells. H69A and H69S cells were collected. (A) Reverse-transcription quantitative PCR analysis of VEGFR, PDGFR, FGFR, c-Kit, Aurora B and CSF1R mRNA levels were assessed using the $2^{-\Delta\Delta Cq}$ method. (B) Phosphorylated mTOR/mTOR were tested by using western blotting. GAPDH was used as the internal standard. (C) Quantitative analysis of (B): H69A was the control (100%). Data are presented as the mean ± the SD of three independent experiments. *P<0.05. VEGFR, vascular endothelial growth factor receptor; PDGFR, platelet-derived growth factor receptor; FGFR, fibroblast growth factor receptors; c-Kit, stem cell factor receptor; CSF1R, colony-stimulating factor 1 receptor; mTOR, mammalian target of rapamycin; p-, phosphorylated.

Treatment-induced stress may induce different subtypes of SCLC interconversion. To investigate whether the selective pressure of therapy would change the SCLC subtypes, these cells were treated with RAD001, anlotinib and CS2164 individually or in combination with chemotherapy [cisplatin + etoposide (EP)]. For RAD001, anlotinib and CS2164, low- and high-concentration experimental groups, respectively, were established. The results were that, after 48 h of drug treatment, YAP1 expression was not significantly altered in low-concentration monotherapy-drug group in H69A and H69S cells (Fig. 4A, C, E and G). The high concentration of RAD001 and the combination treatment group reduced YAP1 by 16 and 17% respectively in H69A and more significantly (41 and 51%, respectively) in H69S (Fig. 4A and C). The high concentration of CS2164 increased YAP1 in H69A cells by 48%, which was significantly higher than that in H69S cells (30%). However, the combination treatment group did not clearly change YAP expression in H69A and H69S cells (Fig. 4E and G). In both phenotypes, ASCL1 expression was not significantly altered in the low-concentration monotherapy group of RAD001 or anlotinib (Fig. 4A, B, E and F), but was decreased in the high-concentration monotherapy group (anlotinib 12% and CS2164 5%), which was lower than that in H69S (43 and 48%; Fig. 4E and F). NEUROD1 expression was increased 14% in high-concentration of CS2164 group in H69A, but decrease 14% in H69S. Moreover, the high concentration of CS2164 combined with EP reduced NEUROD1 by 7% in H69A and more clearly by 33% in H69S (Fig. 4E and H). None of the drugs significantly altered the expression of POU2F3 in the two phenotypes. These results suggest that RAD001, anotinib and CS2164 alone or in combination with EP affect the expression of ASCL1, YAP1 and NEUROD1 with a significant difference between the two phenotypes (Fig. 4A-H).

CSF2 is the main DEG between SCLC adherent and suspended phenotype cells. To explore the molecular mechanism of phenotypic plasticity driving ITH, RNA-seq-based transcriptome profiling analysis was conducted in the H69A and H69S cells and differential expression analysis (expression fold, >1.5) was conducted. In total, 404 DEGs were identified. The heat map analysis indicated that 50.5% of the genes were upregulated and 49.5% were downregulated (Fig. 5A). The GO analysis indicated that these genes were significantly enriched in the nucleosome assembly, chromatin, growth factor activity, protein heterodimerization activity and enzyme activator activity function (Fig. 5B-D). KEGG analysis indicated that these genes were enriched in dysregulated transcriptional signaling pathways in cancer and in the IL-17 signaling pathway (Fig. 5E). These results suggested that DEGs were involved in certain cellular activities associated with types of cancer. Next, the DEGs enriched in KEGG (P<0.05) were selected and the differential genes further screened with log2 (FC)>1.5 or log2 (FC)<-1.5. CSF2 was the only qualified differential gene [P=0.039, log2 (FC)=-1.7796]. CSF2 was significantly enriched in adherent cells, compared to suspension cells. To verify the results of RNA sequencing, the expression levels of the CSF2 gene and proteins in H69A and H69S were detected by using RT-qPCR and western blotting. The expression levels of the CSF2 gene and protein in H69A were higher in H69A cells than in H69S cells (Fig. 5F-H). These results suggested that CSF2 was a major differential gene in SCLC cells of the same clone with different phenotypes.

CSF2 silencing promotes the transition from the adherent phenotype to the suspended phenotype and from the non-NE type to the NE type. CSF2 is involved in the growth, invasion and migration of various tumors such as human melanoma, skin cancer and colorectal cancer (8-9,12). To explore whether CSF2 regulates phenotypic transformation in SCLC, CSF2 was silenced by electroporation in H69A. RT-qPCR and western blotting verified that the cell model was successfully constructed (Fig. 6A-C). It was found that, compared to the control group, the conversion rate of adherent cells to suspension cells increased by 79.57% and cell activity decreased by 24.42% after 48 h of CSF2 silencing (Fig. 6D and E). Furthermore, compared to the control cells, the NE marker

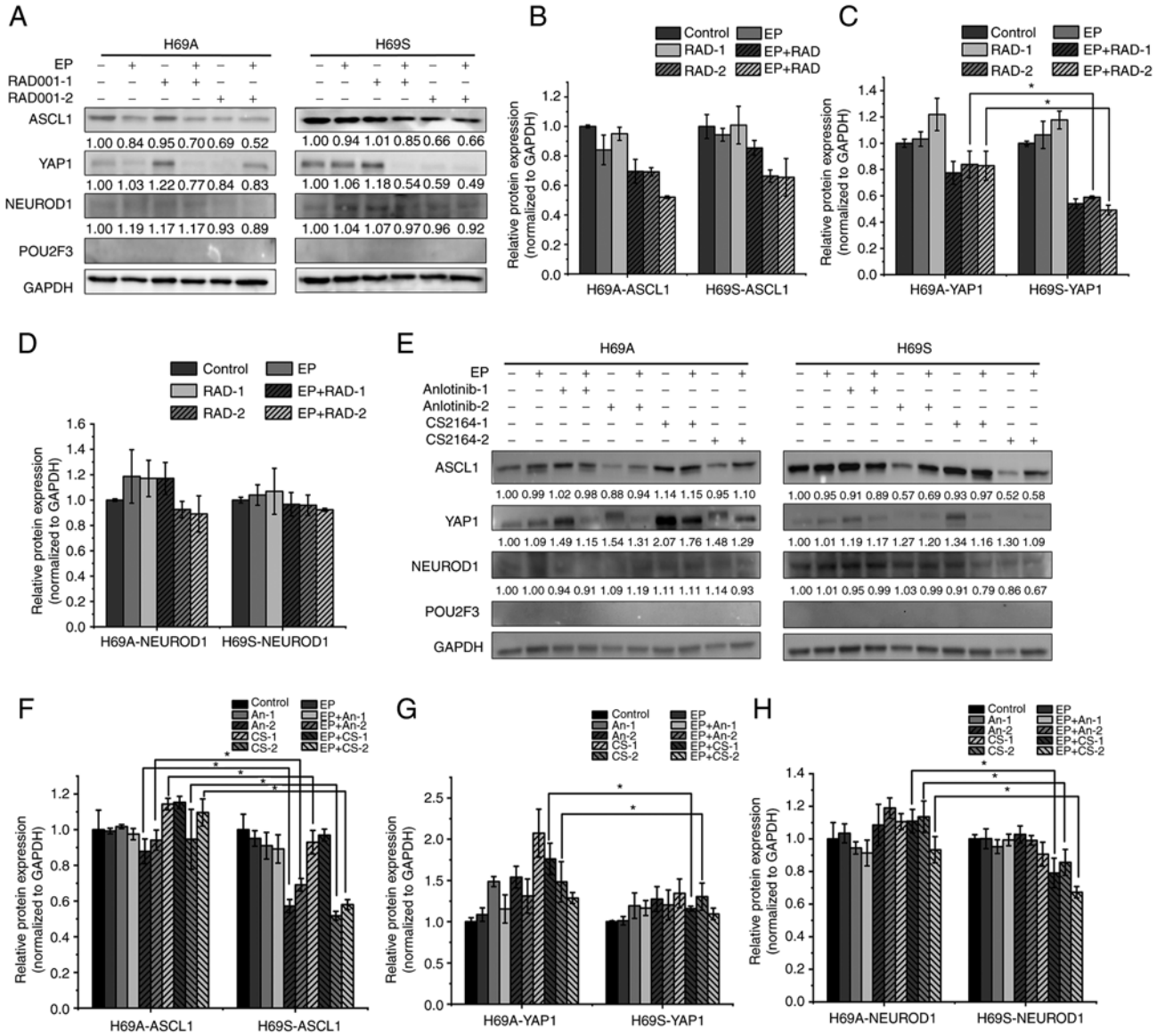

Figure 4. Alternative transcriptional genetic subtypes in H69A and H69S cells. (A) H69A and H69S cells were treated with RAD001 (1 or 8 μg/ml), cisplatin (1 μg/ml) + etoposide (2 μg/ml), or in combination for 48 h. The cells were then harvested and subjected to western blotting analysis using the indicated antibodies. (B-D) Quantitative analysis of (A): mock-treated H69A cells were used as the control. Data are presented as the mean ± the SD of three independent experiments. (E) For 48 h, H69A and H69S cells were treated with cisplatin (1 μg/ml) + etoposide (2 μg/ml), anlotinib (0.5 or 2 μg/ml), CS2164 (0.5 or 2 μg/ml), cisplatin (1 μg/ml) + etoposide (2 μg/ml) + anlotinib (0.5 or 2 μg/ml) and cisplatin (1 μg/ml) + etoposide (2 μg/ml) + CS2164 (0.5 or 2 μg/ml). Western blotting analysis was used to detect the expression of ASCL1, NEUROD1, POU2F3 and YAP1. GAPDH was used as the internal standard. (F-H) Quantitative analysis of (E): mock-treated H69A cells were used as the control (100%). Data are presented as the mean ± standard deviation of three independent experiments. *P<0.05. EP, cisplatin (1 μg/ml) + etoposide (2 μg/ml); ASCL1, achaete-scute homologue 1; NEUROD1, neurogenic differentiation factor 1; POU2F3, POU class 2 homeobox 3; YAP1, YES-associated protein 1; RAD-1, RAD001 1 μg/ml; RAD-2, RAD001 8 μg/ml; An-1, anlotinib 0.5 μg/ml; An-2, anlotinib 2 μg/ml; CS-1, CS2164 0.5 μg/ml; CS-2, CS2164 2 μg/ml.

SYP increased by 36% and the non-NE marker CD44 decreased by 28% in CSF2 knockdown cells (Fig. 6F and G). This finding suggested that the regulation of CSF2 affected the conversion of adherent cells from the same clone to suspension cells, thereby decreasing the number of non-NE SCLC cells and increasing the number of NE-type SCLC cells.

Inhibition of CSF2 increases cell drug sensitivity and the conversion of the non-NE type to the NE type. The CSF2 inhibitor butoconazole nitrate was used to explore the effects of CSF2 on the phenotypic plasticity of SCLC. H69A was treated with butoconazole 24 and 48 h following treatment. As the drug concentration and time increased, cell activity gradually decreased in a dose- and time-dependent manner (Fig. 7A and B). The maximum non-effect dose or minimum toxic dose (7 μg/ml for 24 h and 3 μg/ml for 48 h) at two timepoints was selected to test the inhibitory effect of butoconazole on CSF2. It was found that CSF2 decreased markedly by 30% after 7 μg/ml of butoconazole treatment for 24 h (Fig. 7C and D). H69A cells were then treated with butoconazole nitrate (7 μg/ml for 24 h) combined with anlotinib, CS2164, or RAD001. The results were that, as the combined drug concentration increased, the cell activity gradually decreased in a dose-dependent manner (Fig. 7E-G).

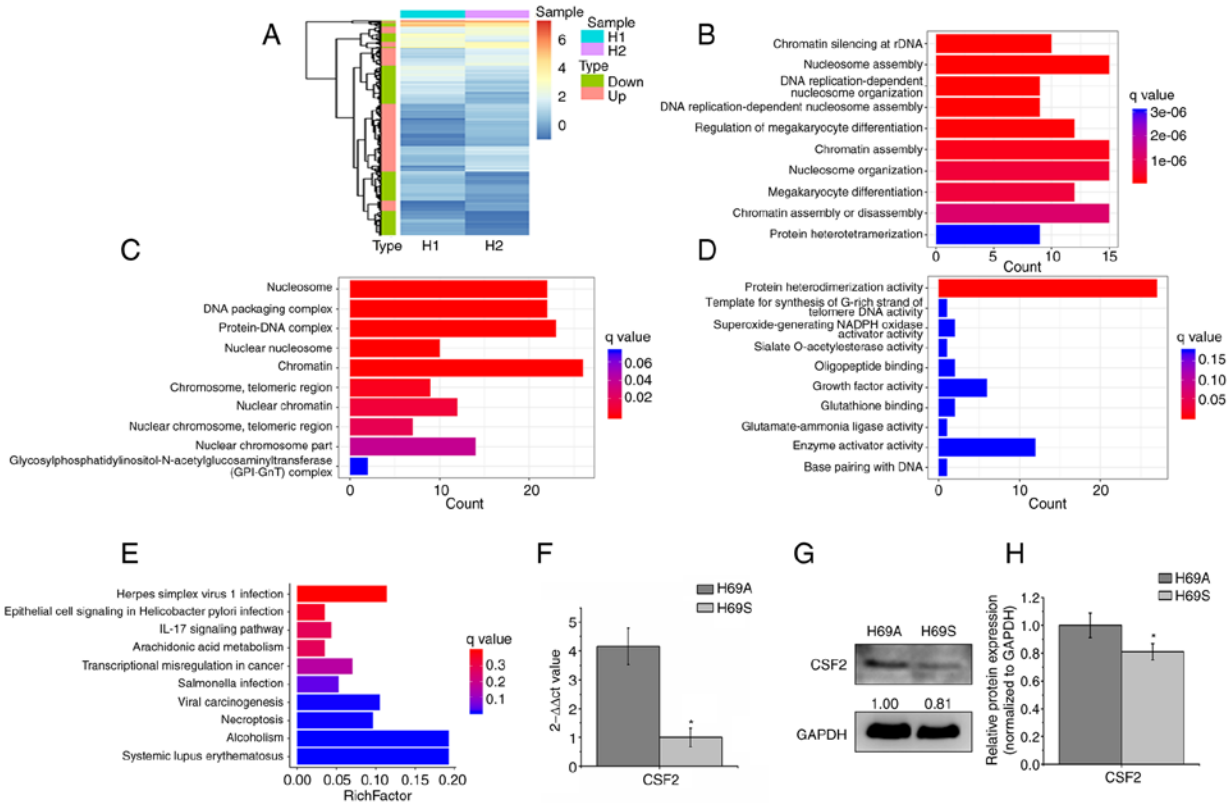

Figure 5. CSF2 is the main difference gene between the adherent and the suspended SCLC phenotypes. H69A and H69S were detected with RNA sequencing. (A) Heat map representation of 404 differentially expressed genes. The significantly enriched GO annotations in (B) Biological Process, (C) Cellular Components and (D) Molecular Function analysis of 404 differentially expressed genes. (E) KEGG pathway analysis of 404 different genes. (F) H69A and H69S cells were collected and CSF2 mRNA levels were evaluated with reverse-transcription quantitative PCR by using the $2^{-\Delta\Delta Cq}$ method. (G) CSF2 was tested by using western blotting. GAPDH was used as the internal standard (*P<0.05, vs. the adherent group). (H) Quantitative analysis of (G): H69A was used as the control (100%). Data are presented as the mean ± standard deviation of three independent experiments (*P<0.05). SCLC, small cell lung cancer; GO, Gene Ontology; KEGG, Kyoto Encyclopedia of Genes and Genomes.

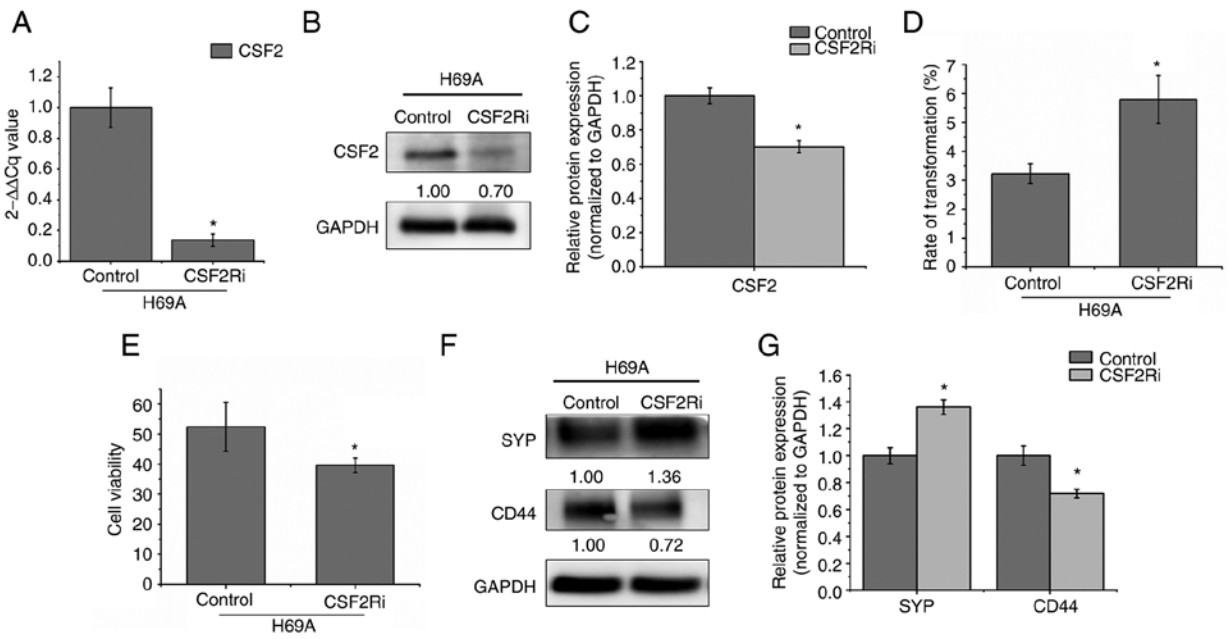

Figure 6. CSF2 silencing inhibits the transformation from the adherent phenotype to the suspension phenotype. H69A was transfected with CSF2 shRNA. (A) The mRNA level of CSF2 was determined using reverse-transcription quantitative PCR. (B) CSF2 protein expression was detected by using western blotting. (C) Quantitative analysis of (B): H69A cells transfected with the control plasmid was used as the control (100%). Data are presented as the mean ± standard deviation of three independent experiments. (D) The conversion rate from the adherent phenotype to the suspended phenotype was detected by using trypan blue staining. (E) Cell viability was detected by using Alamar Blue. (F) The levels of SYP, CD44 and GAPDH were detected by using western blotting (*P<0.05, vs. the control group). (G) Quantitative analysis of (F): H69A cells transfected with the control plasmid were used as the control (100%). Data are presented as mean ± standard deviation of three independent experiments (*P<0.05). CSF2, colony-stimulating factor 2; sh, short hairpin; SYP, synaptophysin.

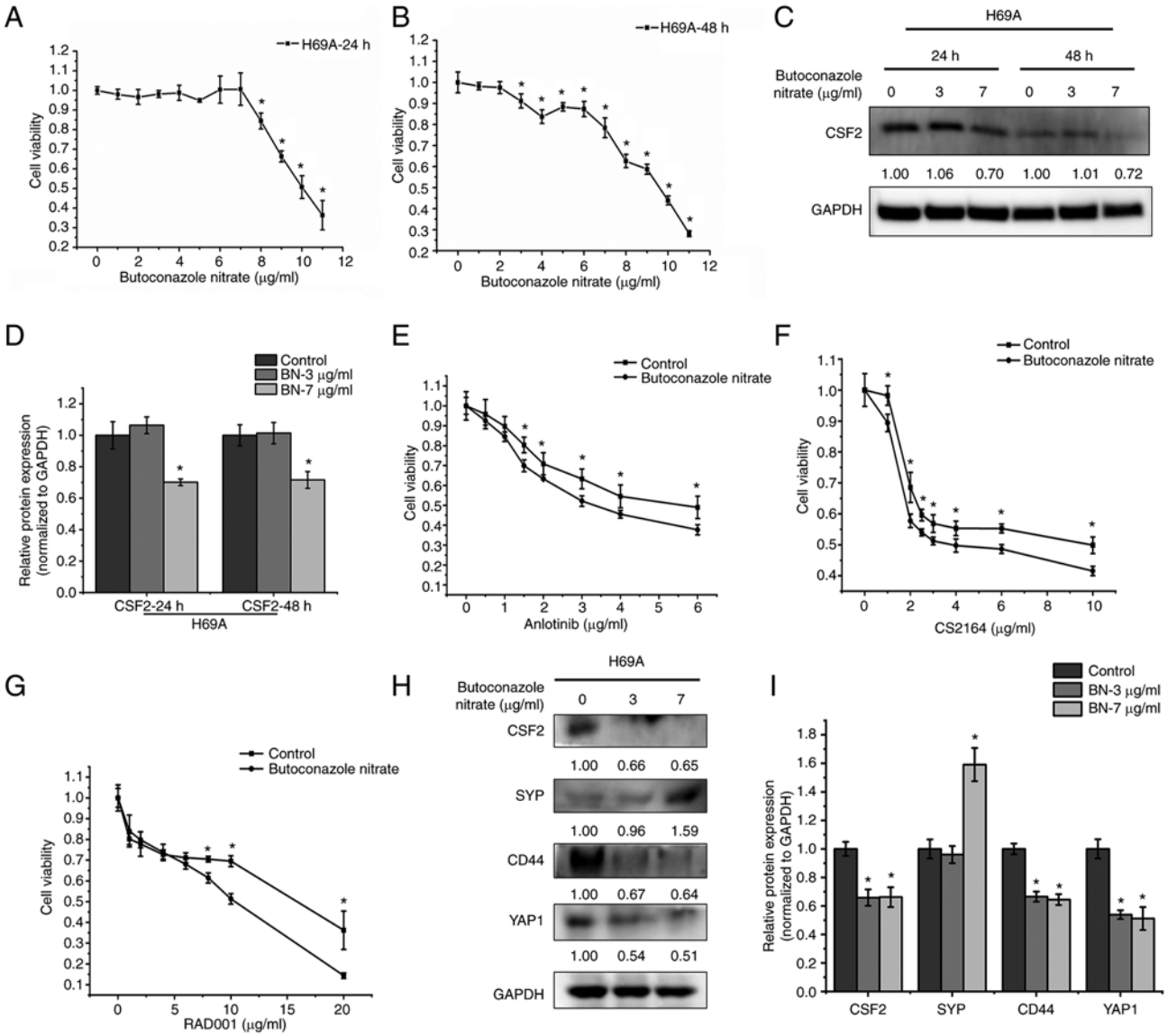

Figure 7. The effect of CSF2 inhibitors on drug sensitivity and the conversion of the non-NE phenotype to the NE phenotype. H69A cells were treated with different concentrations of butoconazole nitrate (0, 1, 2, 3, 4, 5, 6, 7, 8, 9, 10 and 11 μg/ml) and cell viability was detected with Alamar Blue after treatment for (A) 24 h and (B) 48 h. (C) H69A cells treated with 3 and 7 μg/ml butoconazole nitrate. The cells were collected after treatment for 24 and 48 h. The expression of CSF2 and GAPDH were analyzed by using western blotting. (D) Quantitative analysis of (C), mock-treated H69A cells were used as the control (100%). Data are presented as the mean ± standard deviation of three independent experiments. (E) H69A cells were treated with butoconazole nitrate (7 μg/ml) combined with anlotinib (0, 0.5, 1, 1.5, 2, 3, 4 and 6 μg/ml), (F) CS2164 (0, 1, 2, 2.5, 3, 4, 6 and 10 μg/ml) and (G) RAD001 (0, 1, 2, 4, 6, 8, 10 and 20 μg/ml) for 24 h. Cell viability was tested by using Alamar Blue. (H) H69A cells were treated with butoconazole nitrate (3 and 7 μg/ml) for 24 h. Western blotting was used to detect the expression of CSF2, SYP, CD44, YAP1 and GAPDH. (I) Quantitative analysis of (H), mock-treated H69A cells were used as the control (100%). Data are presented as the mean ± standard deviation of three independent experiments. *P<0.05. CSF2, colony-stimulating factor 2; NE, neuroendocrine; CSF2, colony-stimulating factor 2; SYP, synaptophysin; YAP1, YES-associated protein 1.

Compared with anlotinib, CS2164 and RAD001 alone, the combination increased the cell sensitivity to the three drugs (IC_{50}: 4.76 μg/ml vs. 3.46 μg/ml, 5.67 μg/ml vs. 4.57 μg/ml and 23.11 μg/ml vs. 8.23 μg/ml, respectively). H69A cells were then treated with low or high concentrations of butoconazole nitrate. The two concentrations of drugs significantly inhibited CSF2 (34% vs. 35%), CD44 (33% vs. 36%) and YAP1 (46% vs. 49%). A high concentration of butoconazole nitrate strongly increased SYP (59%), but SYP did not change significantly in the low-concentration group (Fig. 7H and I). These results suggested that the inhibition of CSF2 increased the sensitivity to drug treatment and contributes to the transformation of SCLC from the non-NE type to the NE type.

CSF2 regulates phenotypic transformation through p-STAT3/MYC. To further explore the molecular mechanism by which CSF2 can regulate the phenotypic plasticity of SCLC, the present study searched for proteins that could interact with CSF2 through the STRING database. A total of 25 identified proteins were analyzed. CSF2 and STAT3 had a close protein interaction relationship (Fig. 8A). By analyzing the Reactome database, it was found that MYC had a regulatory relationship with STAT3 (Fig. 8B). The Pathway Commons and STRING databases were then searched to analyze the relationship between CSF2, STAT3 and MYC. A regulatory relationship was found between CSF2, STAT3 and MYC (Fig. 8C and D). One report (15) demonstrates that MYC activation induces a

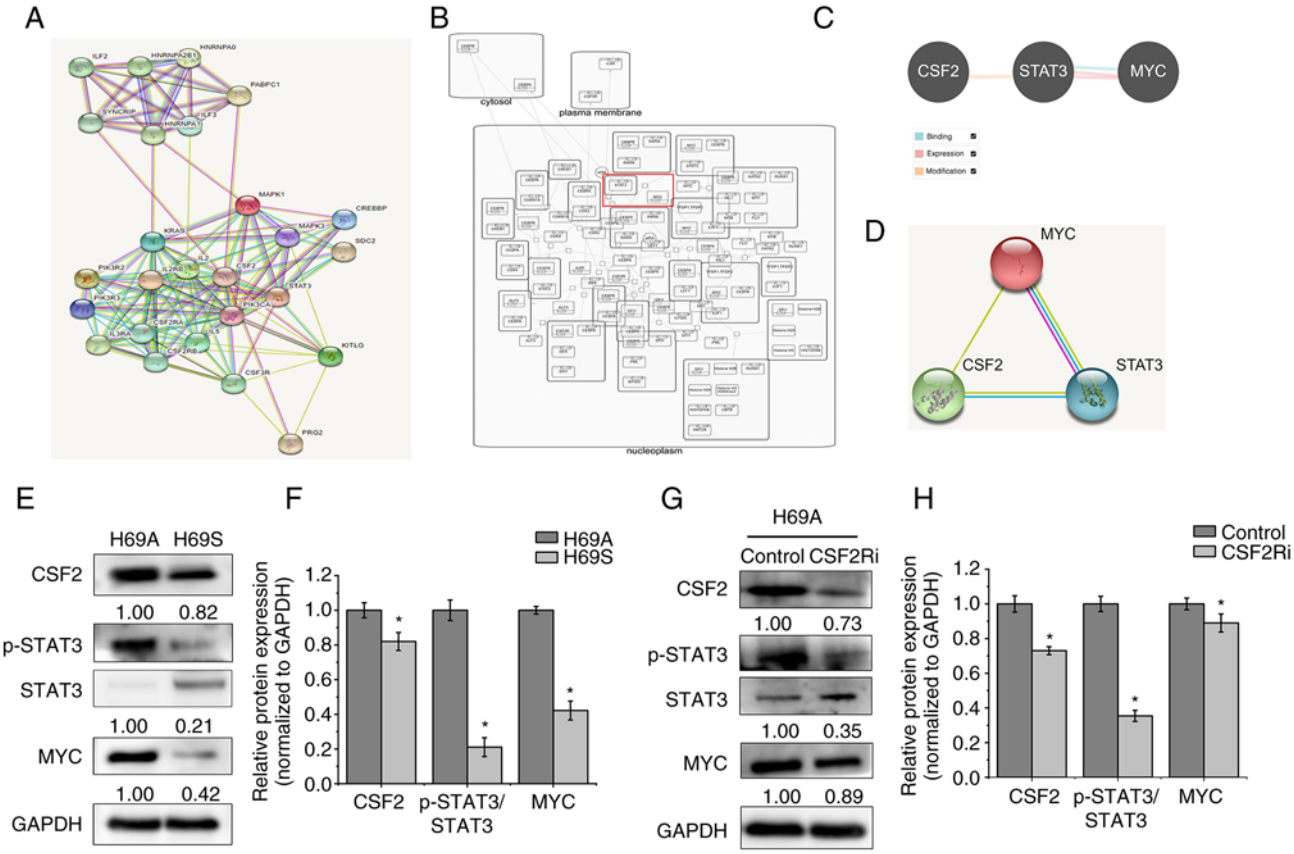

Figure 8. CSF2 regulated phenotypic transformation through p-STAT3/MYC. (A) The STRING database was used to search for proteins that interact with CSF2. Known interactions are indicated with edges of pink (i.e., experimentally determined) and deep sky blue (i.e., database obtained). Predicted interactions are indicated with edges of green (i.e., gene neighborhood), blue (i.e., gene co-occurrence) and red (i.e., gene fusions). Edges of yellow indicate text-mining. Edges of black indicate co-expression. Edges of light purple indicate protein homology. (B) The Reactome database was used to analyze the regulatory relationship between MYC and STAT3. (C) The Pathway Commons database was used to analyze the relationship between CSF2, STAT3 and MYC. The relationship of binding (deep sky blue), expression (pink) and modification (orange) are shown. (D) The STRING database was used to analyze the regulatory relationship between CSF2, STAT3 and MYC. (E) The levels of CSF2, p-STAT3 and MYC in H69A and H69S cells were tested with western blotting. (F) Quantitative analysis of (E): H69A was the control (100%). Data are presented as the mean ± standard deviation of three independent experiments. (G) H69A was transfected with CSF2 shRNA and the expressions of CSF2, p-STAT3, STAT3 and MYC were detected by using western blotting. (H) Quantitative analysis of (G): H69A cells transfected with control plasmid were used as the control (100%). Data are presented as the mean ± standard deviation of three independent experiments. *P<0.05. p-STAT3, phosphorylated signal transducer and activator of transcription 3; CSF2, colony-stimulating factor 2.

shift in SCLC from ASCL1+ to NEUROD1+ to YAP1+ states by reprogramming the NE fate. The CSF2/p-STAT3 signaling pathway promotes epithelial ovarian cancer cell stemness by upregulating MYC (19). Therefore, it was hypothesized that CSF2 regulates phenotypic plasticity in SCLC through the p-STAT3/MYC pathway. The expression of CSF2, p-STAT3 and MYC was detected in H69A and H69S cells and it was found that they were more highly expressed in H69A cells than in H69S cells (Fig. 8E and F). CSF2 silencing significantly reduced the expression of p-STAT3 and MYC in H69A cells (Fig. 8G and H). These results suggested that CSF2 regulates the phenotypic plasticity of SCLC through p-STAT3/MYC.

Discussion

Optimal SCLC treatment has been a challenge for clinicians for nearly three decades. SCLC initially responds well to platinum-based first-line chemotherapy, although drug resistance development usually recurs rapidly (26). The main reason is that the biological characteristics of SCLC have not been clearly identified, including tumor cell origin, tumor evolution and ITH. In practice, the present study found that SCLC cells have genetic differences and phenotypic differences. However, few studies have investigated the biological function and mechanism of phenotypic differences, thus, the objective of the present study.

Intertumor heterogeneity can be studied by microscopic dissection, differences between different tumor sites and samples from different sources (27,28). However, ITH, especially exploration of the function and mechanism of ITH from the same clone source, currently lacks appropriate research models. Single-cell sequencing is an effective means to study clonal evolution and ITH (15,29). However, single cells are difficult to obtain and sequencing is difficult and costly. Lin *et al* (30) established two epidermal growth factor receptor (EGFR) mutant SCLC cell lines from patients with lung adenocarcinoma after failed treatment with the EGFR-tyrosine kinase inhibitor (TKI). They revealed that these SCLC cell lines had two different phenotypes: suspensive and adherent. These two phenotypic cells came from the same origin and could switch back and forth. Compared with suspended cells, adherent cells had higher non-NE characteristics and invasion

capacity (30). The present study found that the adherent and suspended phenotypes of the SCLC cell line NCL-H69 could undergo phenotypic switching and were characterized by specific heterogeneity such as biogenic preference, NE characteristics, cell drug sensitivity and drug target expression. Therefore, NCI-H69 may be a simple and feasible model for exploring the phenotypic plasticity driving ITH.

In non-small-cell lung cancer (NSCLC), DNA-level driver gene mutation typing such as EGFR, anaplastic lymphoma kinase (ALK) and ROS proto-oncogene 1 (ROS1) promotes the long-term survival of patients with NSCLC and lays the foundation for gene-based mutational screening of SCLC (31). Unlike NSCLC, which has clear driving mutations, SCLC is extremely complex with significant heterogeneity in growth pattern, origin, genome expression and copy number changes (5,32). SCLC has obvious characteristics from the standpoint of DNA mutations such as the mutation of P53 and RB deletion, although these DNA gene mutations cannot be used as targets to develop specific targeted drugs or used as features to distinguish between subtypes (33,34). Recent studies (35,36) have demonstrated that several key transcription factors have an important role in the occurrence and development of SCLC through RNA sequencing and that SCLC can be classified, based on transcriptional regulators. Different SCLC subtypes have unique therapeutic vulnerabilities (37-40). Through RNA sequencing, the present study identified CSF2, an important target that drives the phenotypic transition of SCLC and affects the sensitivity of multiple targeted drugs.

Tumor-associated endothelial cells have been reported to secrete cytokines to promote angiogenesis by increasing the expression of cell adhesion molecules (41). CSF2-dependent phosphorylation of JAK2 and STAT3 recruitment are important in tumor angiogenesis and vascularization (42,43). In gliomas, CSF2 can activate antiapoptotic and proangiogenic pathways to promote tumor progression by activating STAT-3 transcription factor or increasing VEGF/VEGFR expression (44-48). Primary and metastatic lung cancers are by far the commonest type of malignant tumor driven by secreted ectopic CSF2 (25,49-51). Microarray data show that CSF2 is enhanced in SCLC, but not in NSCLC (42). In the present study, compared with the SCLC suspension phenotype, CSF2 was expressed at a higher level in adherent SCLC. CSF2 regulated the p-STAT3/MYC signaling pathway to inhibit cell transformation from the adherent type to the suspension type, which was of the same origin in SCLC. Inhibition of CSF2 weakened cell adhesion ability, increased the conversion of adherent phenotypic cells to suspended phenotypic cells and increased the sensitivity of multitarget TKIs with anti-vascular functions. CSF2 is an important target for regulating ITH driven by phenotypic plasticity in SCLC and overcoming drug resistance.

mTOR inhibitors are a targeted therapy approved by the US Food and Drug Administration for some types of cancer, such as NSCLC, breast cancer and pancreatic neuroendocrine neoplasms (52). RAD001, a mTOR inhibitor, unfortunately did not improve outcomes in SCLC clinical trials. This finding may be related to the fact that previous clinical trials did not stratify the enrolled patients (53,54). Anlotinib is a multitarget TKI against VEGFR, FGFR, PDGFR and c-Kit and it suppresses proliferation and induced apoptosis of tumor cells (55,56). Our ALTER1202 study showed that anlotinib monotherapy prolonged progression-free survival and overall survival (OS) in a third-line or later treatment for extensive SCLC (57). Thus, the China Food and Drug Administration approved anlotinib for clinical practice. As stated earlier, whether different SCLC subtypes may achieve different treatment effects with anlotinib is unclear. CS2164 is a highly selective multikinase inhibitor with potent activities against VEGFR, PDGFR, c-Kit, Aurora B and colony-stimulating factor 1 receptor (58) and it inhibits tumor growth by targeting certain key pathways such as tumor mitosis, angiogenesis and the inflammatory microenvironment of the tumor. A Phase I clinical study (59) of CS2164 demonstrates an acceptable safety and favorable pharmacokinetic profile with potential antitumor activity. The current study used three targeted drugs, RAD001, anlotinib and CS2164, which have been marketed or included in clinical studies. It was found that the sensitivity to the three drugs was different in SCLC with different phenotypes, although both phenotypes belonged to the SCLC-A subtype. Even if patients with SCLC belong to the same molecular subtype, differences may exist in antitumor effects. Further stratification of SCLC patients is necessary before treatment.

YAP1 can be activated by the HIPPO signaling pathway (33), is highly expressed in non-NE SCLC (60) and defines a distinct subtype with a T-cell inflamed phenotype in SCLC (61). As a cytokine, CSF2 is primarily involved in the regulation of immune activation and inflammatory factors in the tumor microenvironment (62,63). The present study found that the inhibition of CSF2 reduced non-NE expression and YAP1 expression. It was hypothesized that CSF2 directly regulated the tumor itself and regulated the phenotypic plasticity of SCLC through the tumor microenvironment. The authors of the present study are conducting research in this area. A high level of YAP1 is reported to promote multidrug resistance (4). In the present study, YAP1 expression was the significantly changed following treatment with multiple chemotherapy or targeted drugs. Compared with H69S cells, H69A cells treated with high concentrations of RAD001 had a significantly decreased expression of YAP1. However, high concentrations of CS2164 had a clearly increased expression of YAP1. Therefore, how to select drugs and doses to suppress ITH-driven drug resistance is worth considering when determining the existence of ITH. Ireland *et al* (15) showed that MYC activates Notch signaling during NE dedifferentiation in SCLC on a conserved trajectory from SCLC-A to SCLC-N to SCLC-Y. Their study suggested that the SCLC-A, SCLC-N and SCLC-Y subtypes are different stages of the progressive evolution of SCLC and that the regulation of MYC expression changes cell fate, morphology and drug sensitivity.

Other studies show that the CSF2/p-STAT3 signaling pathway upregulates MYC expression and enhances the stemness of epithelial ovarian cancer cells (19). Inhibition of STAT3 significantly reduces cell adhesion capacity (20) and the expression of the non-NE marker CD44 (21). The present study also found that CSF2, p-STAT3 and MYC may be involved in the regulation of cell phenotypic plasticity. CSF2 inhibition decreased p-STAT3 and MYC expression

and promoted the conversion of adherent cells with relatively low ASCL1 expression and relatively high YAP1 expression to suspension cells with a relatively high ASCL1 expression and relatively low YAP1. Furthermore, because few studies exist on ITH-driven drug resistance, additional studies are warranted to verify the results in clinical specimens such as organoids and we are conducting such research.

In conclusion, the present study confirmed that SCLC with different phenotypes of the same clone can switch between phenotypes and exhibit heterogeneity in cellular viability, drug sensitivity, NE/non-NE characteristics and other aspects. CSF2 is an important target for regulating phenotypic plasticity, which drives ITH. Targeting CSF2 can drive SCLC from the adherent phenotype to the suspended phenotype through the p-STAT3/MYC pathway, thereby making cells more anchored to the suspended phenotype and increasing the expression of the NE marker and the sensitivity of anlotinib, CS2164 and RAD001. The present study identified novel pathways involved in restricting phenotypic plasticity and reducing ITH of SCLC, which is essential for the development of new therapies to control drug resistance and relapse in SCLC.

Acknowledgements

Not applicable.

Funding

The present study was financially supported by the Health and Family Planning Commission of Jilin Province (grant nos. 2021JC095 and 2018J023) and the Development and Reform Commission of Jilin Province (grant nos. 2021C042-7 and 2021C043-1).

Availability of data and materials

The data generated using high-throughput sequencing in this study can be found in the Sequence Read Archive under accession number PRJNA792442 (http://www.ncbi.nlm.nih.gov/sra/PRJNA792442). Other data generated and analyzed during the current study are available from the corresponding author on reasonable request.

Authors' contributions

HL and RZ designed the study and wrote the manuscript. RZ, CH, CT and YL conducted the experiments and acquired the data. HC, RL and SL assisted with data analysis. YL and SL contributed reagents, materials and analytical tools. YC was involved in the conception and design of the study. YC and RZ confirm the authenticity of all the raw data. All authors reviewed and approved the final manuscript.

Ethics approval and consent to participate

Not applicable.

Patient consent for publication

Not applicable.

Competing interests

The authors declare that they have no competing interests.

References

1. Oronsky B, Reid TR, Oronsky A and Carter CA: What's new in sclc? A review. Neoplasia 19: 842-847, 2017.
2. Jahchan NS, Lim JS, Bola B, Morris K, Seitz G, Tran KQ, Xu L, Trapani F, Morrow CJ, Cristea S, *et al*: Identification and targeting of long-term tumor-propagating cells in small cell lung cancer. Cell Rep 16: 644-656, 2016.
3. Nicholson AG, Chansky K, Crowley J, Beyruti R, Kubota K, Turrisi A, Eberhardt WE, van Meerbeeck J, Rami-Porta R; Staging and Prognostic Factors Committee, *et al*: The international association for the study of lung cancer lung cancer staging project: Proposals for the revision of the clinical and pathologic staging of small cell lung cancer in the forthcoming eighth edition of the tnm classification for lung cancer. J Thorac Oncol 11: 300-311, 2016.
4. Song Y, Sun Y, Lei Y, Yang K and Tang R: YAP1 promotes multidrug resistance of small cell lung cancer by CD74-related signaling pathways. Cancer Med 9: 259-268, 2020.
5. Prabavathy D and Ramadoss N: Heterogeneity of small cell lung cancer stem cells. Adv Exp Med Biol 1139: 41-57, 2019.
6. Gazdar AF, Carney DN, Nau MM and Minna JD: Characterization of variant subclasses of cell lines derived from small cell lung cancer having distinctive biochemical, morphological, and growth properties. Cancer Res 45: 2924-2930, 1985.
7. Zhang W, Girard L, Zhang YA, Haruki T, Papari-Zareei M, Stastny V, Ghayee HK, Pacak K, Oliver TG, Minna JD and Gazdar AF: Small cell lung cancer tumors and preclinical models display heterogeneity of neuroendocrine phenotypes. Transl Lung Cancer Res 7: 32-49, 2018.
8. Calbo J, van Montfort E, Proost N, van Drunen E, Beverloo HB, Meuwissen R and Berns A: A functional role for tumor cell heterogeneity in a mouse model of small cell lung cancer. Cancer Cell 19: 244-256, 2011.
9. Sutherland KD, Proost N, Brouns I, Adriaensen D, Song JY and Berns A: Cell of origin of small cell lung cancer: Inactivation of Trp53 and Rb1 in distinct cell types of adult mouse lung. Cancer Cell 19: 754-764, 2011.
10. Quintanal-Villalonga Á, Chan JM, Yu HA, Pe'er D, Sawyers CL, Sen T and Rudin CM: Lineage plasticity in cancer: A shared pathway of therapeutic resistance. Nat Rev Clin Oncol 17: 360-371, 2020.
11. Baldwin GC, Golde DW, Widhopf GF, Economou J and Gasson JC: Identification and characterization of a low-affinity granulocyte-macrophage colony-stimulating factor receptor on primary and cultured human melanoma cells. Blood 78: 609-615, 1991.
12. Lamouille S, Xu J and Derynck R: Molecular mechanisms of epithelial-mesenchymal transition. Nat Rev Mol Cell Biol 15: 178-196, 2014.
13. Chen S, Chen X, Li W, Shan T, Lin WR, Ma J, Cui X, Yang W, Cao G, Li Y, *et al*: Conversion of epithelial-to-mesenchymal transition to mesenchymal-to-epithelial transition is mediated by oxygen concentration in pancreatic cancer cells. Oncol Lett 15: 7144-7152, 2018.
14. Chaffer CL, Marjanovic ND, Lee T, Bell G, Kleer CG, Reinhardt F, D'Alessio AC, Young RA and Weinberg RA: Poised chromatin at the ZEB1 promoter enables breast cancer cell plasticity and enhances tumorigenicity. Cell 154: 61-74, 2013.
15. Ireland AS, Micinski AM, Kastner DW, Guo B, Wait SJ, Spainhower KB, Conley CC, Chen OS, Guthrie MR, Soltero D, *et al*: MYC drives temporal evolution of small cell lung cancer subtypes by reprogramming neuroendocrine fate. Cancer Cell 38: 60-78.e12, 2020.
16. Hong IS: Stimulatory versus suppressive effects of GM-CSF on tumor progression in multiple cancer types. Exp Mol Med 48: e242, 2016.
17. Mueller MM and Fusenig NE: Constitutive expression of G-CSF and GM-CSF in human skin carcinoma cells with functional consequence for tumor progression. Int J Cancer 83: 780-789, 1999.

18. Trutmann M, Terracciano L, Noppen C, Kloth J, Kaspar M, Peterli R, Tondelli P, Schaeffer C, Zajac P, Heberer M and Spagnoli GC: GM-CSF gene expression and protein production in human colorectal cancer cell lines and clinical tumor specimens. Int J Cancer 77: 378-385, 1998.
19. Li X, Wang J, Wu W, Gao H, Liu N, Zhan G, Li L, Han L and Guo X: Myeloid-derived suppressor cells promote epithelial ovarian cancer cell stemness by inducing the CSF2/p-STAT3 signalling pathway. FEBS J 287: 5218-5235, 2020.
20. Qin W, Tian Y, Zhang J, Liu W, Zhou Q, Hu S, Yang F, Lu L, Lu H, Cui S, *et al*: The double inhibition of PDK1 and STAT3-Y705 prevents liver metastasis in colorectal cancer. Sci Rep 9: 12973, 2019.
21. Lin CH, Chiang MC and Chen YJ: STAT3 mediates resistance to anoikis and promotes invasiveness of nasopharyngeal cancer cells. Int J Mol Med 40: 1549-1556, 2017.
22. Li X, Brock GN, Rouchka EC, Cooper NGF, Wu D, O'Toole TE, Gill RS, Eteleeb AM, O'Brien L and Rai SN: A comparison of per sample global scaling and per gene normalization methods for differential expression analysis of RNA-seq data. PLoS One 12: e0176185, 2017.
23. Sahraeian SME, Mohiyuddin M, Sebra R, Tilgner H, Afshar PT, Au KF, Bani Asadi N, Gerstein MB, Wong WH, Snyder MP, *et al*: Gaining comprehensive biological insight into the transcriptome by performing a broad-spectrum RNA-seq analysis. Nat Commun 8: 59, 2017.
24. Livak KJ and Schmittgen TD: Analysis of relative gene expression data using real-time quantitative PCR and the 2(-Delta Delta C(T)) method. Methods 25: 402-408, 2001.
25. Fukutomi T, Kohno M, Izumi Y, Watanabe M, Hayashi Y and Nomori H: Pulmonary pleomorphic carcinoma producing granulocyte-macrophage colony-stimulating factor: Report of a case. Surg Today 42: 288-291, 2012.
26. Rudin CM, Ismaila N, Hann CL, Malhotra N, Movsas B, Norris K, Pietanza MC, Ramalingam SS, Turrisi AT III and Giaccone G: Treatment of small-cell lung cancer: American society of clinical oncology endorsement of the american college of chest physicians guideline. J Clin Oncol 33: 4106-4111, 2015.
27. Giercksky HE, Thorstensen L, Qvist H, Nesland JM and Lothe RA: Comparison of genetic changes in frozen biopsies and microdissected archival material from the same colorectal liver metastases. Diagn Mol Pathol 6: 318-325, 1997.
28. Friedmann-Morvinski D: Glioblastoma heterogeneity and cancer cell plasticity. Crit Rev Oncog 19: 327-336, 2014.
29. Maynard A, McCoach CE, Rotow JK, Harris L, Haderk F, Kerr DL, Yu EA, Schenk EL, Tan W, Zee A, *et al*: Therapy-induced evolution of human lung cancer revealed by single-cell RNA sequencing. Cell 182: 1232-1251.e22, 2020.
30. Lin CA, Yu SL, Chen HY, Chen HW, Lin SU, Chang CC, Yu CJ, Yang PC and Ho CC: EGFR-mutant SCLC exhibits heterogeneous phenotypes and resistance to common antineoplastic drugs. J Thorac Oncol 14: 513-526, 2019.
31. Herbst RS, Morgensztern D and Boshoff C: The biology and management of non-small cell lung cancer. Nature 553: 446-454, 2018.
32. Raso MG, Bota-Rabassedas N and Wistuba II: Pathology and classification of SCLC. Cancers (Basel) 13: 820, 2021.
33. Rudin CM, Poirier JT, Byers LA, Dive C, Dowlati A, George J, Heymach JV, Johnson JE, Lehman JM, MacPherson D, *et al*: Molecular subtypes of small cell lung cancer: A synthesis of human and mouse model data. Nat Rev Cancer 19: 289-297, 2019.
34. George J, Lim JS, Jang SJ, Cun Y, Ozretić L, Kong G, Leenders F, Lu X, Fernández-Cuesta L, Bosco G, *et al*: Comprehensive genomic profiles of small cell lung cancer. Nature 524: 47-53, 2015.
35. Rudin CM, Brambilla E, Faivre-Finn C and Sage J: Small-cell lung cancer. Nat Rev Dis Primers 7: 3, 2021.
36. Gay CM, Stewart CA, Park EM, Diao L, Groves SM, Heeke S, Nabet BY, Fujimoto J, Solis LM, Lu W, *et al*: Patterns of transcription factor programs and immune pathway activation define four major subtypes of SCLC with distinct therapeutic vulnerabilities. Cancer Cell 39: 346-360.e7, 2021.
37. Huang YH, Klingbeil O, He XY, Wu XS, Arun G, Lu B, Somerville TDD, Milazzo JP, Wilkinson JE, Demerdash OE, *et al*: POU2F3 is a master regulator of a tuft cell-like variant of small cell lung cancer. Genes Dev 32: 915-928, 2018.
38. Chalishazar MD, Wait SJ, Huang F, Ireland AS, Mukhopadhyay A, Lee Y, Schuman SS, Guthrie MR, Berrett KC, Vahrenkamp JM, *et al*: MYC-driven small-cell lung cancer is metabolically distinct and vulnerable to arginine depletion. Clin Cancer Res 25: 5107-5121, 2019.
39. Huang F, Ni M, Chalishazar MD, Huffman KE, Kim J, Cai L, Shi X, Cai F, Zacharias LG, Ireland AS, *et al*: Inosine monophosphate dehydrogenase dependence in a subset of small cell lung cancers. Cell Metab 28: 369-382.e5, 2018.
40. Mollaoglu G, Guthrie MR, Böhm S, Brägelmann J, Can I, Ballieu PM, Marx A, George J, Heinen C, Chalishazar MD, *et al*: MYC drives progression of small cell lung cancer to a variant neuroendocrine subtype with vulnerability to aurora kinase inhibition. Cancer Cell 31: 270-285, 2017.
41. Chen C, Duckworth CA, Zhao Q, Pritchard DM, Rhodes JM and Yu LG: Increased circulation of galectin-3 in cancer induces secretion of metastasis-promoting cytokines from blood vascular endothelium. Clin Cancer Res 19: 1693-1704, 2013.
42. Valdembri D, Serini G, Vacca A, Ribatti D and Bussolino F: In vivo activation of JAK2/STAT-3 pathway during angiogenesis induced by GM-CSF. FASEB J 16: 225-227, 2002.
43. Zgheib A, Lamy S and Annabi B: Epigallocatechin gallate targeting of membrane type 1 matrix metalloproteinase-mediated Src and Janus kinase/signal transducers and activators of transcription 3 signaling inhibits transcription of colony-stimulating factors 2 and 3 in mesenchymal stromal cells. J Biol Chem 288: 13378-13386, 2013.
44. Brantley EC, Nabors LB, Gillespie GY, Choi YH, Palmer CA, Harrison K, Roarty K and Benveniste EN: Loss of protein inhibitors of activated STAT-3 expression in glioblastoma multiforme tumors: Implications for STAT-3 activation and gene expression. Clin Cancer Res 14: 4694-4704, 2008.
45. Weissenberger J, Loeffler S, Kappeler A, Kopf M, Lukes A, Afanasieva TA, Aguzzi A and Weis J: Il-6 is required for glioma development in a mouse model. Oncogene 23: 3308-3316, 2004.
46. Niola F, Evangelisti C, Campagnolo L, Massalini S, Buè MC, Mangiola A, Masotti A, Maira G, Farace MG and Ciafrè SA: A plasmid-encoded VEGF siRNA reduces glioblastoma angiogenesis and its combination with interleukin-4 blocks tumor growth in a xenograft mouse model. Cancer Biol Ther 5: 174-179, 2006.
47. Jung KH, Chu K, Lee ST, Kim SJ, Sinn DI, Kim SU, Kim M and Roh JK: Granulocyte colony-stimulating factor stimulates neurogenesis via vascular endothelial growth factor with STAT activation. Brain Res 1073-1074: 190-201, 2006.
48. Ohki Y, Heissig B, Sato Y, Akiyama H, Zhu Z, Hicklin DJ, Shimada K, Ogawa H, Daida H, Hattori K and Ohsaka A: Granulocyte colony-stimulating factor promotes neovascularization by releasing vascular endothelial growth factor from neutrophils. FASEB J 19: 2005-2007, 2005.
49. Lammel V, Stoeckle C, Padberg B, Zweifel R, Kienle DL, Reinhart WH and Simon HU: Hypereosinophilia driven by GM-CSF in large-cell carcinoma of the lung. Lung Cancer 76: 493-495, 2012.
50. Bahar B, Acedil Ayc Iota B, Çoşkun U, Büyükberber S, Benekli M and Yildiz R: Granulocyte colony stimulating factor (G-CSF) and macrophage colony stimulating factor (M-CSF) as potential tumor markers in non small cell lung cancer diagnosis. Asian Pac J Cancer Prev 11: 709-712, 2010.
51. Shalom G, Sion-Vardy N, Dudnik J and Ariad S: Leukemoid reaction in lung cancer patients. Isr Med Assoc J 12: 255-256, 2010.
52. Orr-Asman MA, Chu Z, Jiang M, Worley M, LaSance K, Koch SE, Carreira VS, Dahche HM, Plas DR, Komurov K, *et al*: mTOR kinase inhibition effectively decreases progression of a subset of neuroendocrine tumors that progress on rapalog therapy and delays cardiac impairment. Mol Cancer Ther 16: 2432-2441, 2017.
53. Besse B, Heist RS, Papadmitrakopoulou VA, Camidge DR, Beck JT, Schmid P, Mulatero C, Miller N, Dimitrijevic S, Urva S, *et al*: A phase Ib dose-escalation study of everolimus combined with cisplatin and etoposide as first-line therapy in patients with extensive-stage small-cell lung cancer. Ann Oncol 25: 505-511, 2014.
54. Tarhini A, Kotsakis A, Gooding W, Shuai Y, Petro D, Friedland D, Belani CP, Dacic S and Argiris A: Phase II study of everolimus (RAD001) in previously treated small cell lung cancer. Clin Cancer Res 16: 5900-5907, 2010.
55. Lin B, Song X, Yang D, Bai D, Yao Y and Lu N: Anlotinib inhibits angiogenesis via suppressing the activation of VEGFR2, PDGFRβ and FGFR1. Gene 654: 77-86, 2018.
56. Xie C, Wan X, Quan H, Zheng M, Fu L, Li Y and Lou L: Preclinical characterization of anlotinib, a highly potent and selective vascular endothelial growth factor receptor-2 inhibitor. Cancer Sci 109: 1207-1219, 2018.

57. Cheng Y, Wang Q, Li K, Shi J, Liu Y, Wu L, Han B, Chen G, He J, Wang J, *et al*: Anlotinib vs placebo as third- or further-line treatment for patients with small cell lung cancer: A randomised, double-blind, placebo-controlled phase 2 study. Br J Cancer 125: 366-371, 2021.
58. Zhou Y, Shan S, Li ZB, Xin LJ, Pan DS, Yang QJ, Liu YP, Yue XP, Liu XR, Gao JZ, *et al*: CS2164, a novel multi-target inhibitor against tumor angiogenesis, mitosis and chronic inflammation with anti-tumor potency. Cancer Sci 108: 469-477, 2017.
59. Sun Y, Yang L, Hao X, Liu Y, Zhang J, Ning Z and Shi Y: Phase I dose-escalation study of chiauranib, a novel angiogenic, mitotic, and chronic inflammation inhibitor, in patients with advanced solid tumors. J Hematol Oncol 12: 9, 2019.
60. Pearsall SM, Humphrey S, Revill M, Morgan D, Frese KK, Galvin M, Kerr A, Carter M, Priest L, Blackhall F, *et al*: The rare YAP1 subtype of SCLC revisited in a biobank of 39 circulating tumor cell patient derived explant models: A brief report. J Thorac Oncol 15: 1836-1843, 2020.
61. Owonikoko TK, Dwivedi B, Chen Z, Zhang C, Barwick B, Ernani V, Zhang G, Gilbert-Ross M, Carlisle J, Khuri FR, *et al*: YAP1 expression in SCLC defines a distinct subtype with T-cell-inflamed phenotype. J Thorac Oncol 16: 464-476, 2021.
62. Hamilton JA: GM-CSF in inflammation. J Exp Med 217: e20190945, 2020.
63. Mehta HM, Malandra M and Corey SJ: G-CSF and GM-CSF in neutropenia. J Immunol 195: 1341-1349, 2015.